International Journal of Minerals, Metallurgy and Materials
Volume 24, Number 1, January 2017, Page 64
DOI: 10.1007/s12613-017-1379-4

Influence of mill scale and rust layer on the corrosion resistance of low-alloy steel in simulated concrete pore solution

Jin-jie Shi and Jing Ming

Jiangsu Key Laboratory of Construction Materials, School of Materials Science and Engineering, Southeast University, Nanjing 211189, China
(Received: 14 June 2016; revised: 23 September 2016; accepted: 26 September 2016)

Abstract: Electrochemical impedance spectroscopy, cyclic potentiodynamic polarization measurements, and scanning electron microscopy in conjunction with energy-dispersive X-ray spectroscopy were used to investigate the influence of mill scale and rust layer on the passivation capability and chloride-induced corrosion behaviors of conventional low-carbon (LC) steel and low-alloy (LA) steel in simulated concrete pore solution. The results show that mill scale exerts different influences on the corrosion resistance of both steels at various electrochemical stages. We propose that the high long-term corrosion resistance of LA steel is mainly achieved through the synergistic effect of a gradually formed compact, adherent and well-distributed Cr-enriched inner rust layer and the physical barrier protection effect of mill scale.

Keywords: steel reinforced concrete; low alloy steel; low carbon steel; steel corrosion; corrosion resistance

1. Introduction

The corrosion of reinforcing steel is one of the most dominant factors affecting the durability of reinforced concrete structures (RCSs) [1–2]. Therefore, conventional low-carbon (LC) steel may no longer meet the requirements of service-life design of RCSs, especially in severe marine environments. Various methods have been adopted to mitigate steel corrosion and to prolong the service life of RCSs. Among them, the use of corrosion-resistant steels is considered a very promising method [3–6]. Low-alloy (LA) steel is a type of coating-free reinforcing steel prepared by adding various trace alloying elements (Cr, Cu, Ni, etc.) during the hot-rolling process. LA steel is expected to exhibit optimal anti-corrosion performance but with much lower cost compared to traditional stainless steels [3,7–9].

In practice, reinforcing steels are embedded in concrete with mill scale. However, to reduce the variability of the results of experiments, the mill scale is often removed from the surface by sandblasting, polishing, or pickling. However, in cases where experiments are conducted to determine the service life of RCSs, any surface modification of the steel surface, especially for the removal of mill scale, should be avoided [10–11]. At present, research concerning the mill scale of steel is mainly focused on the following three aspects.

(1) The corrosion initiation stage. This stage is generally related to the influence of mill scale on the chloride-depassivation threshold (chloride threshold level) [12–17]. Kouřil *et al.* [12] found that mill scale was detrimental to the corrosion resistance of stainless steel, which they attributed to the formation of Cr-depleted mill scale. Therefore, stainless steel without mill scale is generally recommended for use in concrete [3,12]. In the case of conventional LC steel, previous studies revealed that mill scale on the steel surface substantially reduced the chloride threshold level as well [13–16]. However, the results of Pillai and Trejo [17] indicated that the effect of mill scale on the chloride threshold level was mainly dependent on the compactness, homogeneity, and adhesion of the mill scale.

(2) The early corrosion propagation stage. The evolution of the corrosion rate of steel in the absence or presence of mill scale has been frequently discussed [18–21]. Previous studies related to the effects of mill scale on the corrosion rate of still are contradictory. Poursaee and Hansson [18] and Manera *et al.* [19] showed that the corrosion rate of

Corresponding author: Jin-jie Shi E-mail: jinjies@126.com

sand-blasted steel (without mill scale) was substantially lower than that of as-received steel (with mill scale). However, Li and Sagüés [14] arrived at the opposite conclusion.

(3) The corrosion propagation stage. This issue concerns the relationship between the mill scale and the rust layer [20–22]. Most of the mill scales on steel surfaces in concrete or mortar have been demonstrated to be loose and with interconnected microcracks and defects [21–22]. It was confirmed that the presence of porous mill scale could delay the onset of corrosion on steel; however, it does not prevent it [21]. In addition, the corrosion products might accumulate and swell in the crevices between the steel substrate and the mill scale, which is the main reason for the spalling of mill scale [21–22], in good agreement with the results for steel tested in simulated concrete pore solutions [16].

On the basis of the aforementioned literature results, the compactness and adhesion of the mill scale strongly influence the steel corrosion behavior at the corrosion initiation stage as well as during the corrosion propagation stage. However, the literature contains few studies focused on the relationship between mill scale and rust layers and their synergistic effects on the corrosion behavior of LA steel.

In this study, the passivation and corrosion behaviors of LC steel and LA steel with and without mill scale were investigated using electrochemical measurements in simulated concrete pore solution. The influence of mill scale on the distribution of different rust layers was also extensively studied.

2. Exp erimental

2.1. Materials and specimen preparation

The LA steel with trace corrosion-resistant alloying elements was specially designed to replace the conventional LC steel. Both steels were air-cooled to ensure that mill scale formed under the same conditions. The chemical compositions of the LC steel and the LA steel are shown in Table 1. The LA steel contains 0.859wt% Cr and a very small amount of alloying elements Cu and Ni compared to the amount of these elements in the LC steel. The Cr content in the LA steel is far lower than that in stainless steel, which makes the LA steel substantially less expensive [3]. To improve the plasticity and weldability, the carbon content in LA steel is relatively lower than that in LC steel. In addition, the relatively low carbon content in LA steel is expected to minimize the possible formation of chromium carbide, which is detrimental to the improvement of corrosion resistance [23]. The mechanical properties of the LA steel, which include a tensile strength of 650 MPa, a yield strength of 450 MPa, and a total elongation of 31%, are comparable to those of conventional LC steel.

Table 1. Chemical composition of the investigated steels wt%

Steel type	Fe	C	Si	Mn	P	S	V	Cr	Cu	Ni
LC	Bal.	0.220	0.530	1.440	0.0250	0.0220	0.0380	—	—	—
LA	Bal.	0.199	0.654	0.571	0.0267	0.0076	0.0323	0.859	0.056	0.033

Fig. 1 shows the optical micrographs of the microstructures of the LC and LA steels after they were etched in 4% nital solution (4 mL HNO_3 mixed with 96 mL ethanol). The optical micrographs of both the LC and the LA steels show two dominant phases — brighter ferrite and darker pearlite (a combination of ferrite and carbide) — which is the typical microstructure for conventional LC reinforcing steel [24]. In addition, the grain size of the LA steel (Fig. 1(b)) is slightly larger than that of the LC steel (Fig. 1(a)) because different heat treatment processes were used when Cr was added. The addition of ferritizer element Cr results in a high transformation temperature for the LA steel. Thus, it promotes the growth of ferrite grains at high-temperature zones.

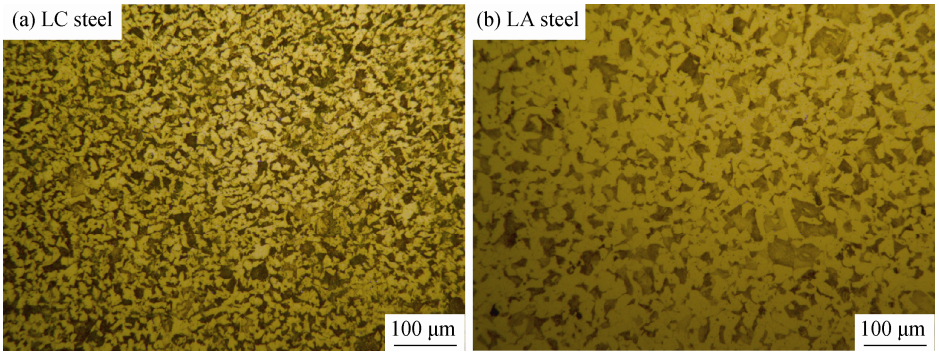

Fig. 1. Optical microscopy images of the LC and LA steels.

Fig. 2 shows the microstructure of the mill scale. Wrinkles are observed for the mill scale of the LA steel (Fig. 2(b)), which could affect the formation of a stable passive film. In the case of the cross-sections of the mill scale, microcracks are observed in the mill scale of the LC steel (Fig. 2(c)). However, as shown in Fig. 2(d), the mill scale of LA steel is more compact than that of the LC steel.

The steel specimens were cut into 40-mm segments with a diameter of 20 mm. A central hole was drilled on the top of each steel specimen, and a copper wire was attached to the top end of each specimen (Fig. 3(a)), similar to the steel specimens prepared by Ghods *et al.* [10]. The steel specimens were cleaned with alcohol prior to being coated with epoxy resin at both ends. To mitigate or avoid crevice corrosion, the interface of the steel substrate and the epoxy resin coating was carefully sealed. The middle part of each steel specimen, with an exposure area of approximately 12.57 cm^2, was then exposed to simulated solutions (Fig. 3(a)). These specimens met the requirements for steel specimens proposed by Li and Sagüés [25].

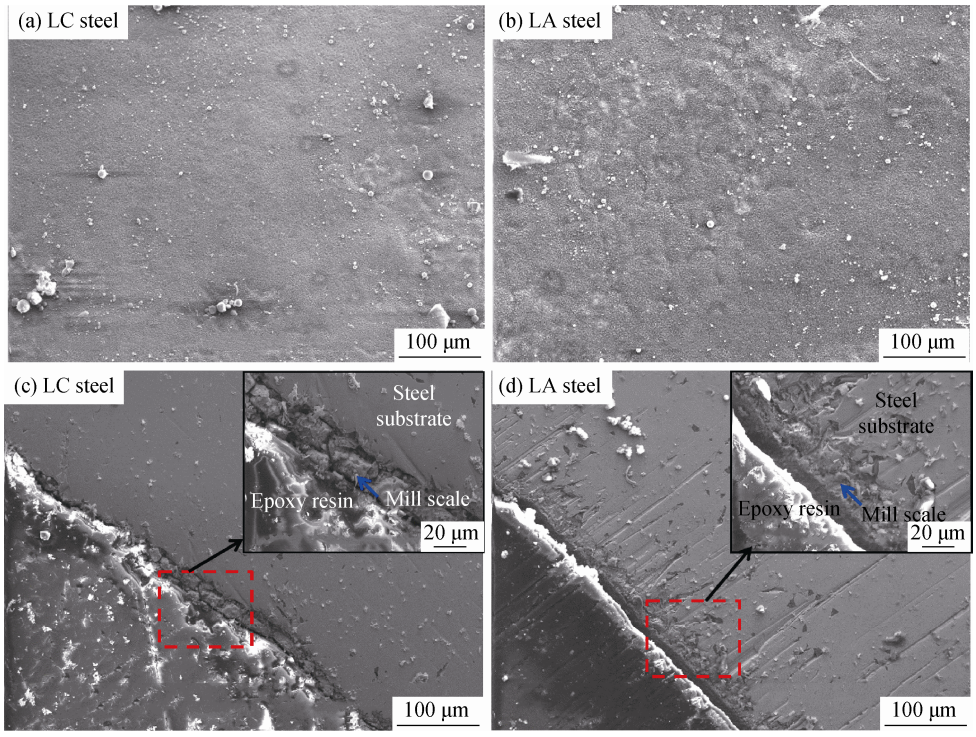

Fig. 2. SEM images of the surface morphology (a,b) and cross-section morphology (c,d) of mill scale.

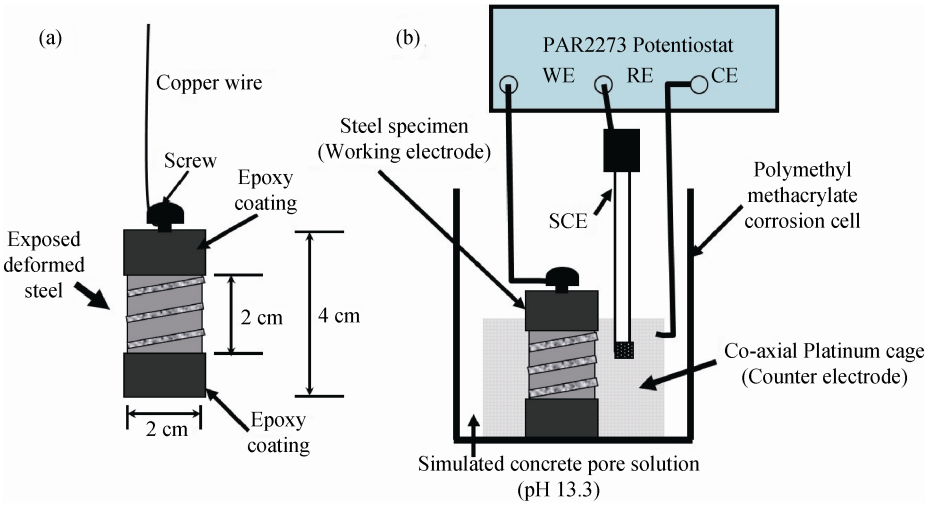

Fig. 3. Schematic of a steel specimen (a) and a three-electrode corrosion cell (b).

In this study, four different conditions for steel specimens were investigated: sand-blasted LC, as-received LC, sand-blasted LA, and as-received LA. Each condition had six duplicate steel specimens, three steel specimens were used to conduct cyclic potentiodynamic polarization (CPP) measurements, and the other three steel specimens were used in long-term corrosion experiments in a simulated concrete pore solution (SCPS).

2.2. Electrochemical measurements

The SCPS used herein was 0.1 M NaOH + 0.2 M KOH + 0.1 M $Ca(OH)_2$ + 0.003 M $CaSO_4$ with a pH value of 13.3 at room temperature [10]. All reagents used in the solutions were of analytical grade, and deionized water (18 MΩ·cm) was used as the solvent. A solution volume of 400 mL was used in each corrosion cell to ensure a minimum ratio of 0.2 mL/mm^2 between the solution volume and the specimen surface area [26]. During the experiments, the corrosion cells were covered with a PMMA lid to mitigate the carbonation of the SCPS.

All steel specimens were cleaned with alcohol and then dried prior to immersion in SCPS. The three-electrode corrosion cell is shown in Fig. 3(b). A PAR 2273 potentiostat was used to conduct the electrochemical measurements. A steel specimen was used as the working electrode. The saturated calomel electrode (SCE) and co-axial platinum cage electrode were used as the reference electrode and the counter electrode, respectively.

Electrochemical impedance spectroscopy (EIS) was conducted at stable open-circuit potentials with an AC perturbation amplitude of 10 mV in the frequency range from 100 kHz to 10 mHz. The EIS data were fitted using the ZSimpWin software. CPP curves were measured from 100 mV negative to corrosion potential (E_{corr}) up to 100 mV vs. SCE, and then reversed to E_{corr}. The scan rate of CPP was 1 mV/s. All the potentials mentioned herein were referred to the saturated calomel electrode (SCE). All experiments were conducted at room temperature ((25 ± 1)°C).

The electrochemical process of steels in SCPS was divided into three stages: (1) the passivation stage in chloride-free SCPS (2 h to 7 d); (2) the stage of stepwise addition of NaCl (0.05 M NaCl per day from 8 d to 27 d) to depassivate the passive film [14]; (3) the stage of the evolution of corrosion products at a constant NaCl concentration of 1.0 M (28 d to 87 d).

2.3. Microstructural characterization

After the electrochemical measurements, steel specimens were sectioned in the transverse orientation with respect to the drawing direction and then cast into a low-viscosity epoxy resin to minimize any artificial damage. The microstructures and composition of the rust layers and mill scale in the cross sections of samples were characterized by SEM and energy-dispersive X-ray spectroscopy (EDS). All SEM images and EDS analyses (line and area scans of the characteristic elements) were obtained on a Philips XL30 environmental scanning electron microscope in backscattered electron (BSE) mode.

3. Results and discussion

3.1. Electrochemical behavior

3.1.1. Electrochemical impedance spectroscopy

Fig. 4 shows the representative Bode plots for sand-blasted LC and LA steels in SCPS with various chloride concentrations. The impedance moduli (Figs. 4(a) and 4(b)) and absolute maximum phase angles (Figs. 4(c) and 4(d)) of the sand-blasted LC and LA steels largely increase after 7 d of passivation in chloride-free SCPS. These behaviors are attributed to the formation of a protective passive film on a steel surface. As the NaCl concentration in SCPS was increased to 0.5 M (17 d), the impedance moduli and absolute maximum phase angles for both the sand-blasted LC and the sand-blasted LA steel decrease sharply. These behaviors indicate the depassivation of passive films and the occurrence of active corrosion. When the NaCl concentration was increased to 1.0 M in 27 d, the corrosion resistance of the sand-blasted LC and LA steels continued to decrease to different degrees. These results indicate that both steels had entered the stage of stable active corrosion; similar corrosion resistances were observed. Notably, the selection of 1.0 M as the endpoint NaCl concentration in the SCPS was based on the research by Moser *et al.* [26]. The chloride concentration remained unchanged until 87 d (1.0 M), and a notable decrease in the corrosion resistance appeared again, as shown in Fig. 4.

In general, the number of capacitive arcs in Nyquist plots and the peaks of the phase angle in Bode plots are associated with the number of time constants, although the time constants tend to overlap each other in some cases [27–29]. Notably, in Figs. 4(c) and 4(d), both sand-blasted LC and LA steels exhibit only one time constant of 2 h. However, after passivation and active corrosion, the Bode plots show another time constant, which is attributable to the presence of a passive film and corrosion products on the steel surface, respectively [27].

The Bode plots of the as-received LC and LA steels are presented in Fig. 5. Two time constants are observed for both the passivation and the corrosion stage. Fig. 5 shows that the impedance moduli (Figs. 5(a) and 5(b)) for both steels unexpectedly decrease after 7 d of passivation in chloride-free SCPS. Notably, the passivation behaviors of steels

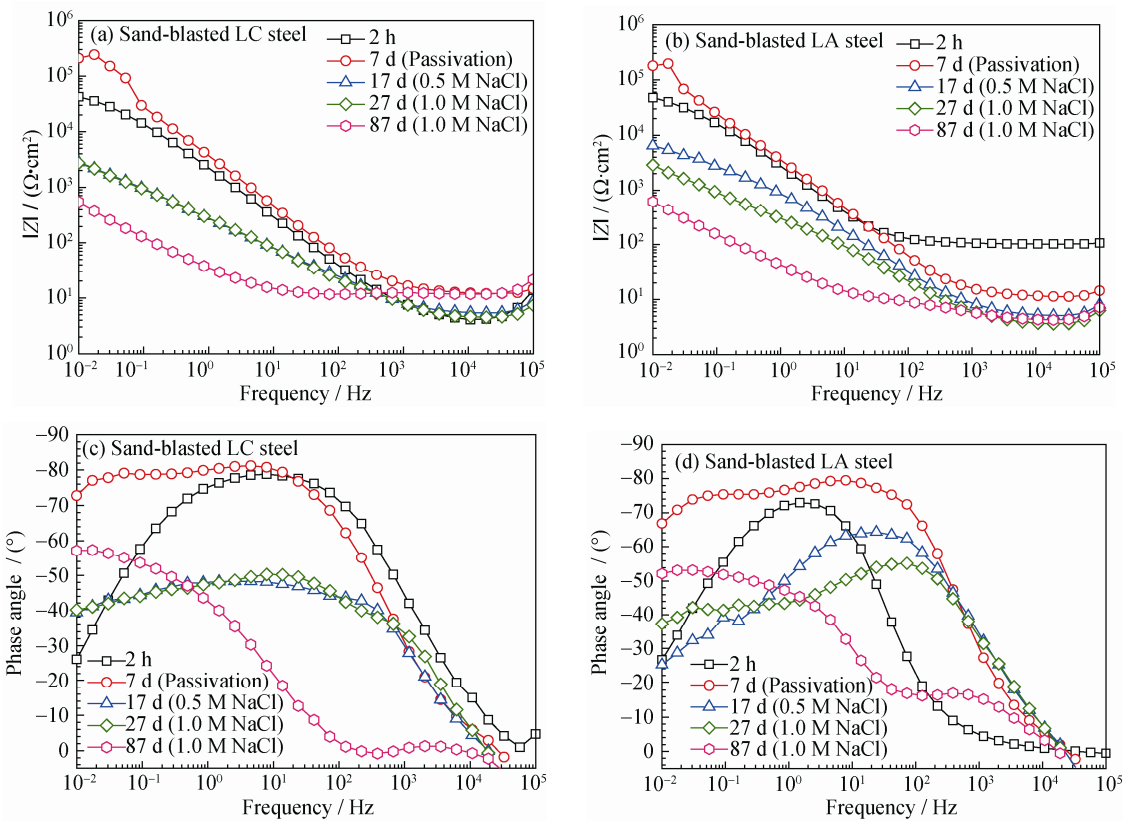

Fig. 4. Representative Bode plots of sand-blasted steels at various exposure times in SCPS: (a,b) impedance plots; (c,d) phase angle plots.

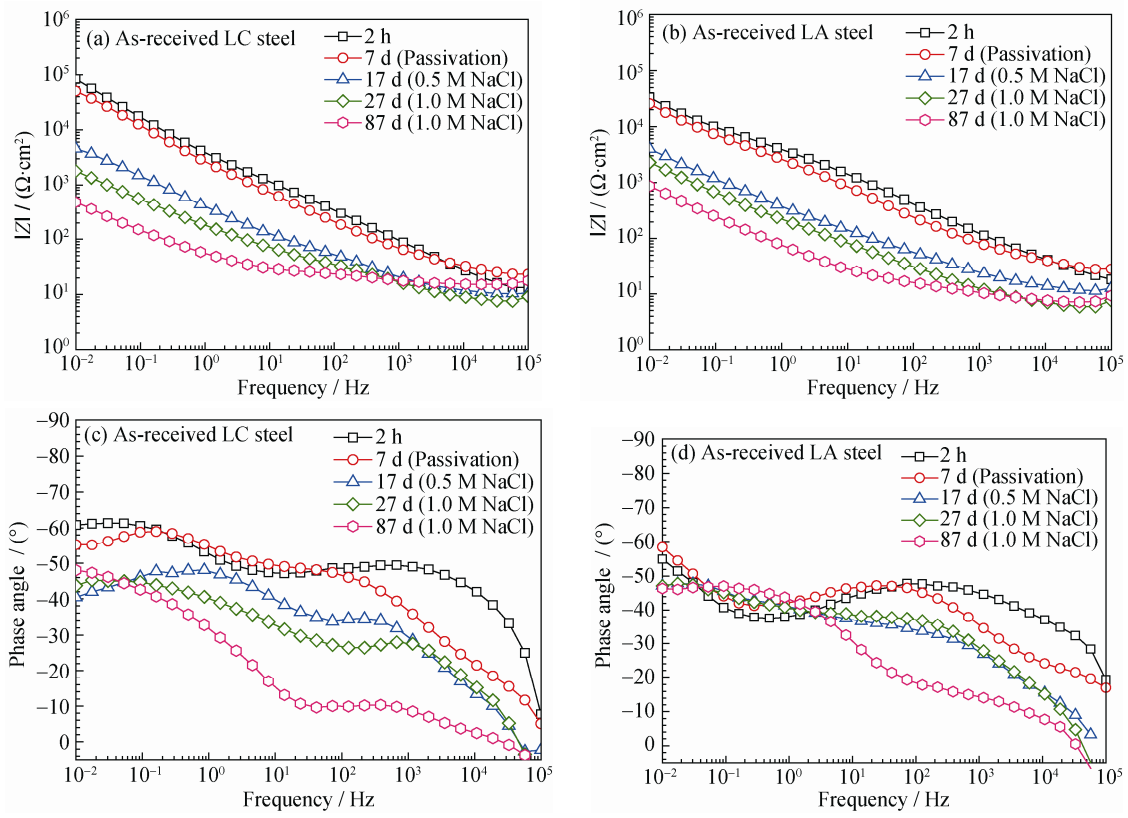

Fig. 5. Representative Bode plots of as-received steels at various exposure times in SCPS: (a,b) impedance plots; (c,d) phase angle plots.

in the presence of mill scale substantially differ from those under the conditions without mill scale, as shown in Fig. 4. A possible explanation for this phenomenon is the different microstructures. The sand-blasted steels exhibit homogeneous and smooth surfaces with few microcracks and defects, facilitating the formation of a dense and protective passive film. By contrast, the surface of the as-received steels contains several crevices and defects due to the presence of loose mill scale (Fig. 2). Moreover, atmospheric corrosion has inevitably occurred on the surface of the mill scale during transportation and storage of the steels. As a consequence, the formation of a protective passive film on the surface of the mill scale is difficult and the corrosion resistance of the as-received steels is even lower after passivation.

Various equivalent electric circuits (EECs) have been used to interpret the impedance spectra for steel under passive and active corrosion conditions [27]. In this study, two generally used EECs for steels in SCPSs are shown in Fig. 6. Only one time constant is evident in EEC1 (Fig. 6(a)); we used this time constant to fit the impedance spectra for the sand-blasted LC steel and the sand-blasted LA steel at 2 h.

Fig. 6(b) presents EEC2 with two time constants for fitting the impedance spectra of steels collected under other conditions. In Fig. 6, the constant phase element (CPE, expressed as Q) is used as an alternative to the pure capacitor to represent the non-homogeneity of a steel surface. It mainly arises from defects and the precipitation of corrosion products on the steel surface. In EEC1, R_s is the resistance of the SCPS, the time constant $R_{ct}Q_{dl}$ refers to the double-layer capacitance (Q_{dl}) at the steel–solution interface and the charge transfer resistance (R_{ct}) of the steel. In EEC2, $R_{ct}Q_{dl}$ is the low-frequency time constant. The high-frequency time constant $R_{ox}Q_{ox}$ is associated with the redox reactions (Fe^{2+}/Fe^{3+}) of the passive film and/or the corrosion products [27–29]. R_{ox} and Q_{ox} are the resistance and capacitance, respectively, of the passive film and/or the corrosion products.

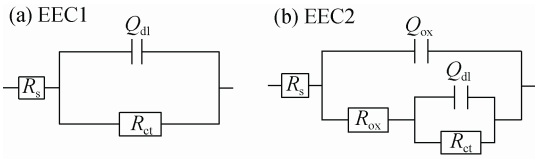

Fig. 6. Proposed equivalent electric circuits (EECs) for fitting the impedance spectra.

Fig. 7 presents the average fitted R_{ct} values and standard deviation for triplicate LC and LA steels at different exposure times. After 7 d of pre-passivation in chloride-free SCPS (Fig. 7(a) and 7(b)), the R_{ct} values of sand-blasted

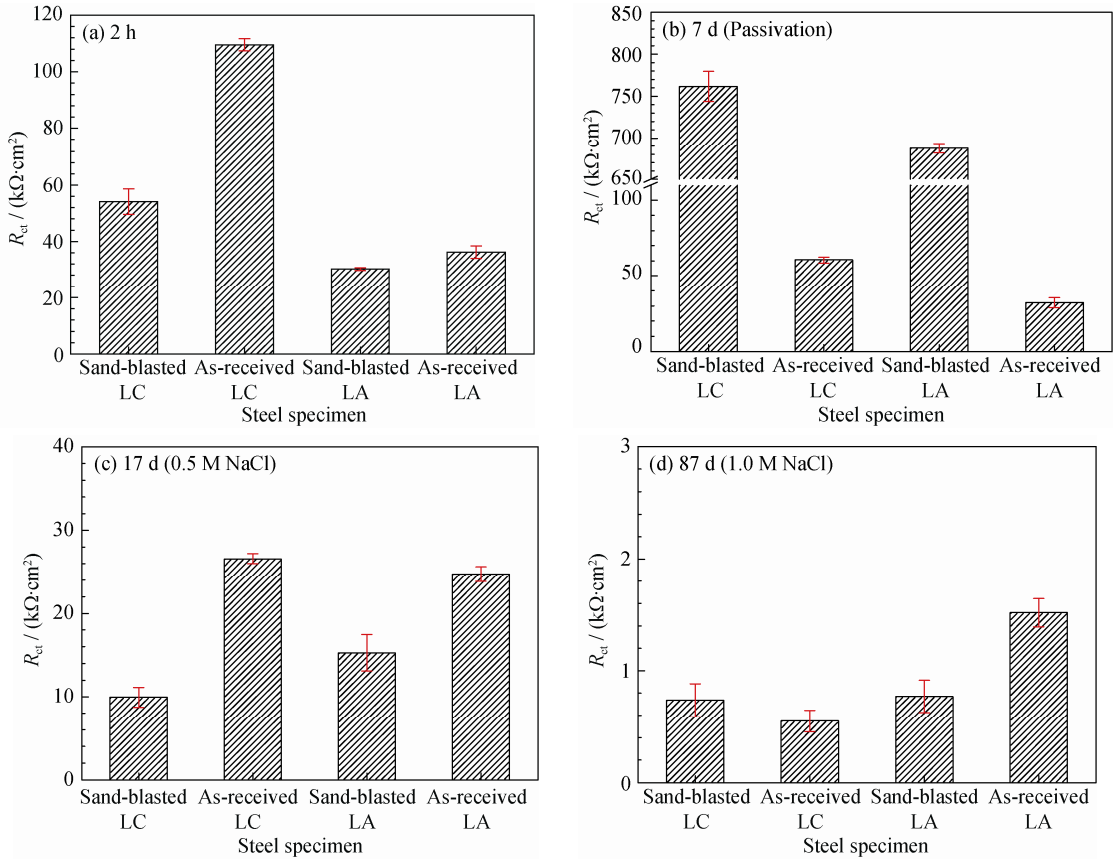

Fig. 7. Average R_{ct} values for triplicate steels at different exposure times in SCPSs with incrementally increasing NaCl content.

steels increased by approximately one order of magnitude, confirming the formation of the protective passive film on the steel surface. Contrarily, the R_{ct} values of the as-received steels showed a slightly decreasing trend after passivation. These results indicate that no stable and protective passive film was formed on the steel surface in the presence of mill scale or that an unstable and defective passive film was formed. Consequently, the mill scale inhibits or delays the formation of a protective passive film, irrespective of whether the steel is LC steel or LA steel [13–16].

The R_{ct} values for all steels tended to decrease when the concentration of NaCl in the SCPS was increased to 0.5 M (Fig. 7(c)). However, R_{ct} values for the sand-blasted steels decreased to a much larger extent than those for the as-received steels, consistent with the results of Li and Sagüés [14]. Fig. 7(c) shows that the R_{ct} values for the as-received steels are slightly higher than those for the sand-blasted steels at 0.5 M NaCl. As a result, we inferred that the presence of mill scale on steel surfaces can mitigate the corrosion activity at the early corrosion propagation stage. At the end of the immersion tests (Fig. 7(d)), as-received LA steel exhibited the highest R_{ct} value, which was almost double that of the as-received LC steel.

3.1.2. Cyclic potentiodynamic polarization

The CPP curves for the LC and LA steels in SCPSs with 0.5 M NaCl are presented in Fig. 8. For the LC steels (Fig. 8(a)), almost the same electrochemical behavior is identified upon anodic polarization at potentials greater than E_{corr}. At a polarization potential of approximately −0.05 V vs. SCE, a sudden increase of the current density for both steels was observed, suggesting the emergence of pitting corrosion. When the anodic polarization potential reached 0.1 V vs. SCE, the backward potential scan was performed. The corresponding current density of the backward potential scan for both LC steels was remarkably higher than that of the forward scan; a positive hysteresis loop then formed, indicating the development of corrosion pits on the steel surface. The area enclosed within such hysteresis loops is generally used to quantify the pitting corrosion behavior. A larger area represents a lower pitting corrosion resistance [26]. Although both LC steels presented almost the same E_{pit} value, the area of the hysteresis loop for the as-received LC steel was substantially smaller than that for the sand-blasted LA steel, indicating that the anodic dissolution rate of the as-received LC steel within the pits was relatively lower [30].

The pitting corrosion behaviors for LA steels are shown in Fig. 8(b), which shows that the pitting corrosion resistance for the as-received LA steel was also slightly higher than that for the sand-blasted LA steel, as indicated by the higher E_{pit} value and smaller area of hysteresis loop for the as-received LA steel.

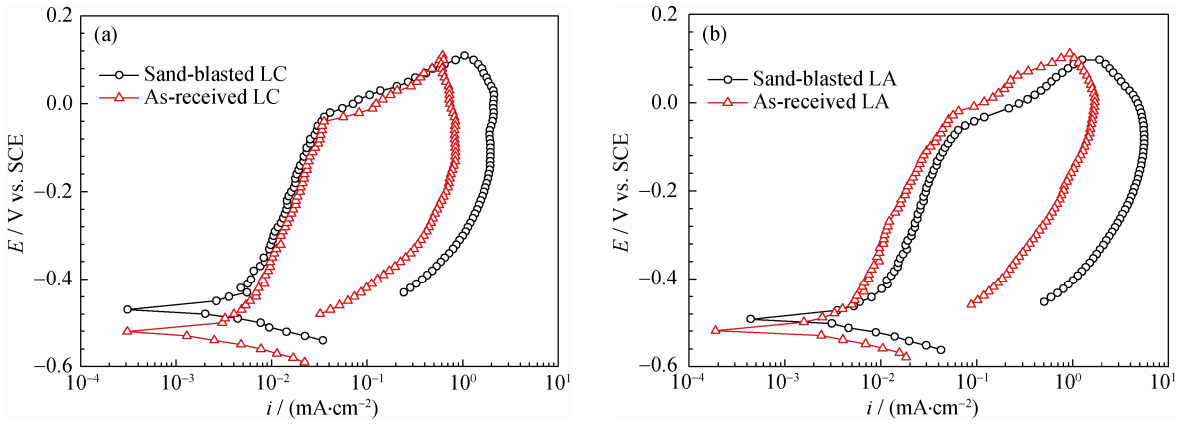

Fig. 8. Cyclic potentiodynamic polarization curves of the LC and LA steels in SCPS containing 0.5 M NaCl.

3.2. Distribution of rust layers

Fig. 9 presents the microstructure characterization of the rust layers on the cross-sections of steels; the EDS line profiles of the characteristic elements in the rust layers are shown in Fig. 10. The surface of the sand-blasted LC steel was covered with a non-uniform rust layer with an average thickness of approximately 10 μm (Fig. 9(a)). In addition, the rust layer was relatively loose and contained several microcracks. The rust layer of the sand-blasted LA steel was relatively thinner and more compact in comparison to that of the sand-blasted LC steel (Fig. 9(b)). Notably, the sand-blasted LA steel contained a small amount of alloying element Cr. The intensity of Cr shows a general trend of gradual decrease when it is close to the region of epoxy resin (Fig. 10(b)).

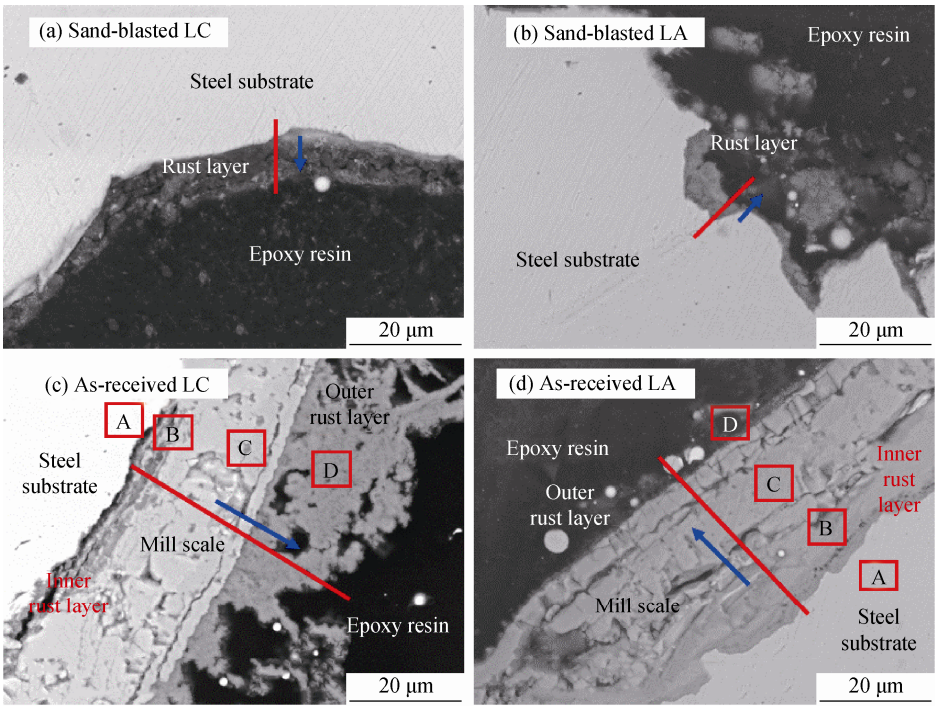

Fig. 9. SEM images of the cross-section morphology of steels in SCPS containing 1.0 M NaCl (87 d).

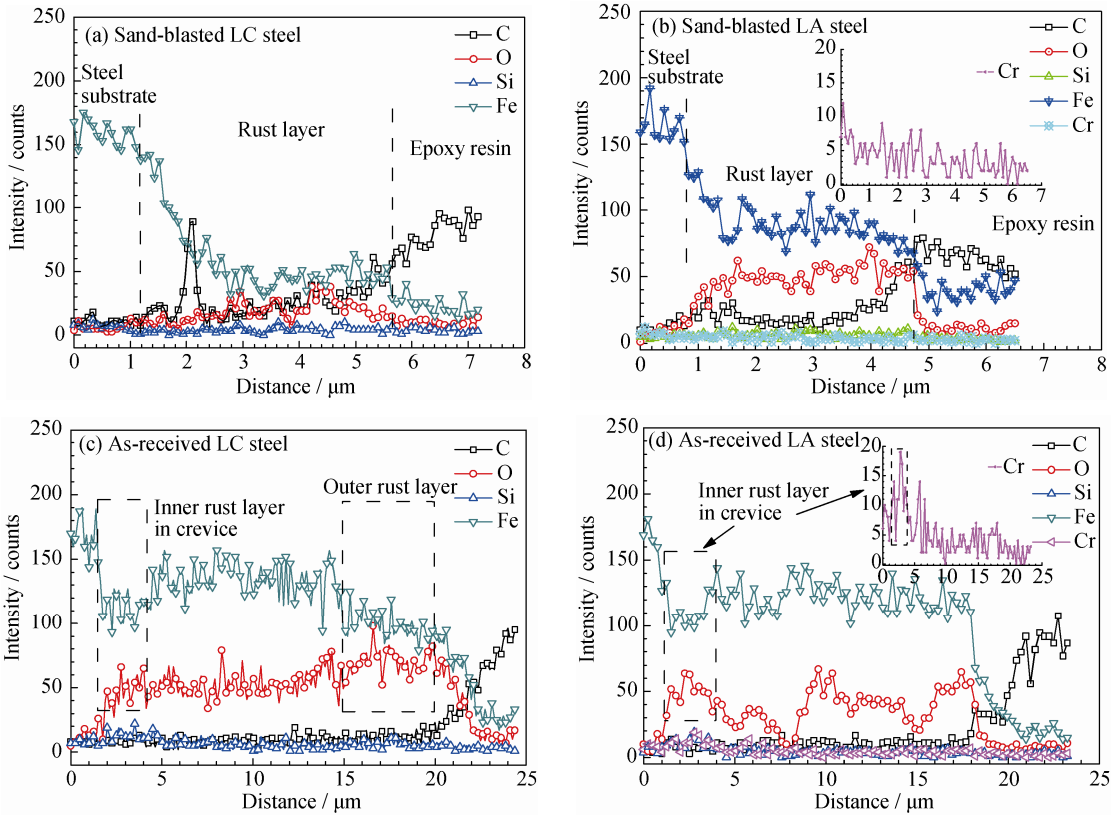

Fig. 10. EDS line profile of characteristic elements for the cross-sections of steels in SCPS containing 1.0 M NaCl (87 d).

Fig. 9(c) shows that the thickness of the mill scale of the as-received LC steel was approximately 20 μm. The mill scale is full of microcracks and voids, consistent with the results in Fig. 2(c). Furthermore, crevices partially filled

with loose inner rust layer are detected between steel substrate and mill scale. Therefore, the mill scale of the as-received LC steel does not completely adhere to the steel substrate, thereby providing pathways for chloride ions to penetrate into the crevices through the interconnected microcracks in the mill scale. This chloride-ion penetration may be the primary reason for the initiation of crevice corrosion between the steel substrate and the mill scale, in good agreement with the results of Ghods *et al.* [16]. Fig. 10(c) depicts EDS line profiles of the characteristic elements in the cross-section of the as-received LC steel. The inner rust layer and outer rust layer are well distinguished by the intensities of elements Fe and O.

The thickness of the mill scale of the as-received LA steel (Fig. 9(d)) is very similar to that of the as-received LC steel. Although the crevices can also be observed in as-received LA steel, they have been totally filled with inner rust layer. Unlike the as-received LC steel, the inner rust layer in the as-received LA steel is much more compact and adherent, thus effectively preventing further attack of the steel substrate by chloride ions. The EDS line profile of the characteristic elements in the cross-sections of the as-received LA steel (Fig. 10(d)) reveals that, in the region of the inner rust layer, the intensity of element Fe exhibits a decreasing trend, accompanied by an increase in the intensity of element O. In addition, one noteworthy intensity peak of element Cr is displayed in the region of the inner rust layer, demonstrating the enrichment of alloying element Cr and the formation of Cr-enriched corrosion products in the crevices. The phenomenon of the filling effect with a compact and adherent inner rust layer is in good agreement with the results in Fig. 9(d). In previous investigations [31–32], the potential of Cr in the rust layer was lower than the potential of Fe, and Fe in the corrosion product α-FeOOH was then partially replaced by the enriched alloying element Cr. Therefore, a more compact corrosion product, α-$Fe_xCr_{1-x}OOH$ was gradually formed, which provided much better protection of the steel substrate against corrosion.

The distribution of the characteristic elements in the selected regions of the as-received steels in Figs. 9(c) and 9(d) is shown in Fig. 11. The steel substrate, inner rust layer, mill scale, and outer rust layer correspond to selected regions A, B, C, and D in Fig. 9, respectively. Fig. 11(b) clearly shows that the content of element Cr in the inner rust layer of the as-received LA steel is the highest. As expected, the intensity of Cr in the mill scale is substantially lower than that in the inner rust layer and steel substrate, reflecting the depletion of Cr in the mill scale [12].

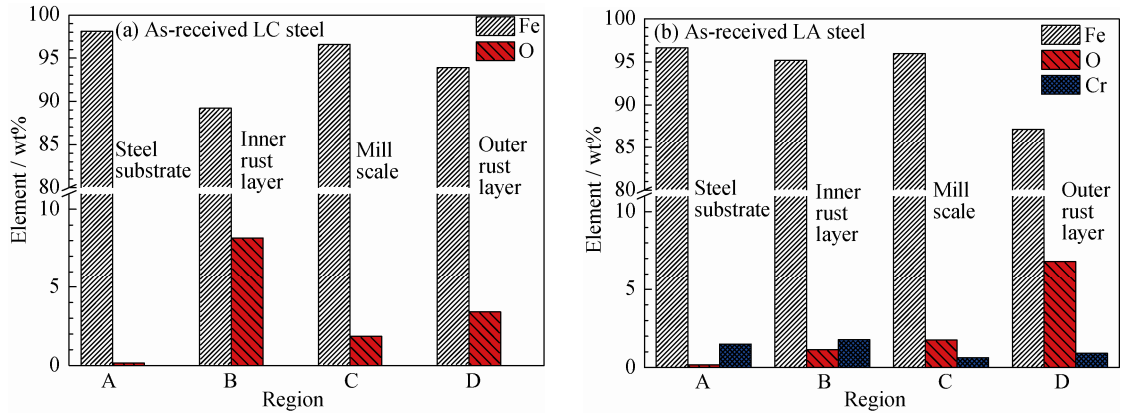

Fig. 11. EDS area scanning of characteristic elements for the cross-sections of the as-received steels in SCPS containing 1.0 M NaCl (87 d).

Passive films are widely acknowledged to vitally affect the depassivation process of steels, especially stainless steels [12,27,33]. However, the aforementioned results (Figs. 9–11) demonstrate that the inner rust layer, rather than the passive film, beneficially affects the corrosion resistance of LA steel. The corrosion resistance of the passive film for the LA steel in this study shows less pronounced improvement compared to that for the LC steel, as shown in Fig. 7(b); this better effect in the case of the LA steel is presumably related to its low content of alloying element Cr and large grain size [34]. Therefore, if the content of Cr is lower than a certain threshold value, the formation of a protective passive film on the steel surface is thought to be difficult, which may strongly affect the initial corrosion resistance of the steel. The content of Cr has been reported to remarkably affect the passivation capability of weathering steel under atmospheric environment [34] and the corrosion resistance of Cr-bearing steel in concrete [7]. When the surface of the LA steel substrate is well-distributed with a certain amount of corrosion products after long-term exposure, the nature of

the rust layer plays the dominant role in determining corrosion resistance (Figs. 9−11) [8].

3.3. Role of mill scale for LA steel

Fig. 7 highlights that, for both steels, the mill scale exerts different influences on the corrosion resistance during different electrochemical stages. At the passivation stage, mill scale inhibits the formation of a passive film (Fig. 7(b)), whereas mill scale on steel surface can mitigate the corrosion activity at the early corrosion propagation stage, as shown in Fig. 7(c).

The results in Figs. 9(d) and 10(d) indicate that the crevices between the steel substrate and the mill scale in the case of LA steel are properly filled with a compact and adherent inner rust layer, which is enriched in alloying element Cr. Fig. 7(d) also shows that, at the end of long-term exposure to SCPS, the corrosion resistance of the sand-blasted LA steel is inferior to that of the as-received LA steel. The reasonable explanation for the diminishing corrosion resistance of sand-blasted LA steel is the partial dissolution of a Cr-enriched rust layer during long-term exposure to SCPS with high chloride ions in the absence of mill scale. Indeed, comparing the peak intensity of Cr in the inner rust layer from Fig. 10(b) with that in Fig. 10(d) reveals that the peak intensity of Cr in the inner rust layer for the as-received LA steel is strongly higher than that in the inner rust layer of the sand-blasted LA steel. This result means that the mill scale serves as a physical barrier against the dissolution of the Cr-enriched inner rust layer for LA steel in SCPS. Therefore, the physical barrier protection effect of mill scale and the filling effect of the compact and adherent inner rust layer provide synergistic benefits for the corrosion resistance of the as-received LA steel.

4. Conclusions

(1) Mill scale exerts different influences on the corrosion resistance of LC and LA steels at different stages. At the passivation stage, mill scale substantially inhibits the passivation process. However, mill scale can mitigate the corrosion activity at the early corrosion propagation stage. Furthermore, CPP measurements indicated that the pitting corrosion process can be delayed to a certain extent by mill scale in SCPS containing 0.5 M NaCl.

(2) The predominant reason for the high corrosion resistance of the as-received LA steel after long-term exposure is the filling effect of the compact and adherent Cr-enriched rust layer in the crevices, rather than the formation of a more protective passive film. Moreover, the barrier protection effect of mill scale for the inner rust layer should also be taken into account.

Acknowledgements

The authors greatly acknowledge the support by the National Natural Science Foundation of China (Nos.51208098 and 51678144), the National Basic Research Program of China (No. 2015CB655100), the Natural Science Foundation of Jiangsu Province (No. BK20161420) and Industry–University Research Cooperative Innovation Fund of Jiangsu Province (No. BY2013091).

References

[1] R. Vera, M. Villarroel, A.M. Carvajal, E. Vera, and C. Ortiz, Corrosion products of reinforcement in concrete in marine and industrial environments, *Mater. Chem. Phys*., 114(2009), No. 1, p. 467.

[2] S.A. Alghamdi and S. Ahmad, Service life prediction of RC structures based on correlation between electrochemical and gravimetric reinforcement corrosion rates, *Cem. Concr. Compos*., 47(2014), p. 64.

[3] F. Presuel-Moreno, J.R. Scully, and S.R. Sharp, Literature review of commercially available alloys that have potential as low-cost, corrosion-resistant concrete reinforcement, *Corrosion*, 66(2010), No. 8, p. 086001.

[4] J.Y. Zhong, M. Sun, D.B. Liu, X.G. Li, and T.Q. Liu, Effects of chromium on the corrosion and electrochemical behaviors of ultra high strength steels, *Int. J. Miner. Metall. Mater.*, 17(2010), No. 3, p. 282.

[5] Q.H. Zhao, W. Liu, J.W. Yang, Y.C. Zhu, B.L. Zhang, and M.X. Lu, Corrosion behavior of low alloy steels in a wet–dry acid humid environment, *Int. J. Miner. Metall. Mater*., 23(2016), No. 9, p. 1076.

[6] S.T. Wang, S.W. Yang, K.W. Gao, and X.L. He, Corrosion behavior and corrosion products of a low-alloy weathering steel in Qingdao and Wanning, *Int. J. Miner. Metall. Mater.*, 16(2009), No. 1, p. 58.

[7] S.H. Tae and T. Ujiro, Corrosion resistance of Cr-bearing rebar in simulated concrete pore solutions, *ISIJ Int.*, 47(2007), No. 9, p. 1324

[8] J.K. Singh and D.D.N. Singh, The nature of rusts and corrosion characteristics of low alloy and plain carbon steels in three kinds of concrete pore solution with salinity and different pH, *Corros. Sci.*, 56(2012), p. 129.

[9] J.J. Shi, W. Sun, J.Y. Jiang, and Y.M. Zhang, Influence of chloride concentration and pre-passivation on the pitting corrosion resistance of low-alloy reinforcing steel in simulated concrete pore solution, *Constr. Build. Mater.*, 111(2016), No. 5, p. 805.

[10] P. Ghods, O.B. Isgor, G.A. McRae, and G.P. Gu, Electrochemical investigation of chloride-induced depassivation of

black steel rebar under simulated service conditions, *Corros. Sci*., 52(2010), No. 5, p. 1649.

[11] L.T. Mammoliti, L.C. Brown, C.M. Hansson, and B.B. Hope, The influence of surface finish of reinforcing steel and pH of the test solution on the chloride threshold concentration for corrosion initiation in synthetic pore solutions, *Cem. Concr. Res*., 26(1996), No. 4, p. 545.

[12] M. Kouřil, P. Novák, and M. Bojko, Threshold chloride concentration for stainless steels activation in concrete pore solutions, *Cem. Concr. Res*., 40(2010), No. 3, p. 431.

[13] E. Mahallati and M. Saremi, An assessment on the mill scale effects on the electrochemical characteristics of steel bars in concrete under DC-polarization, *Cem. Concr. Res*., 36(2006), No. 7, p. 1324.

[14] L. Li and A.A. Sagüés, Chloride corrosion threshold of reinforcing steel in alkaline solutions: open-circuit immersion tests, *Corrosion*, 57(2001), No. 1, p. 19.

[15] T.U. Mohammed and H. Hamada, Corrosion of steel bars in concrete with various steel surface conditions, *ACI Mater. J.*, 103(2006), No. 4, p. 233.

[16] P. Ghods, O.B. Isgor, G.A. McRae, J. Li, and G.P. Gu, Microscopic investigation of mill scale and its proposed effect on the variability of chloride-induced depassivation of carbon steel rebar, *Corros. Sci.,* 53(2011), No. 3, p. 946.

[17] R.G. Pillai and D. Trejo, Surface condition effects on critical chloride threshold of steel reinforcement, *ACI Mater. J*., 102(2005), No. 2, p. 103.

[18] A. Poursaee and C. Hansson, Reinforcing steel passivation in mortar and pore solution, *Cem. Concr. Res*., 37(2007), No. 7, p. 1127.

[19] M. Manera, Ø. Vennesland, and L. Bertolini, Chloride threshold for rebar corrosion in concrete with addition of silica fume, *Corros. Sci*., 50(2008), No. 2, p. 554.

[20] A. Demoulin, C. Trigance, D. Neff, E. Foy, P. Dillmann, and V. L'Hostis, The evolution of the corrosion of iron in hydraulic binders analysed from 46- and 260-year-old buildings, *Corros. Sci*., 52(2010), No. 10, p. 3168.

[21] S.J. Jaffer and C.M. Hansson, Chloride-induced corrosion products of steel in cracked-concrete subjected to different loading conditions, *Cem. Concr. Res*., 39(2009), No. 2, p. 116.

[22] Y.X. Zhao, Y.Y. Wu, and W.L. Jin, Distribution of millscale on corroded steel bars and penetration of steel corrosion products in concrete, *Corros. Sci*., 66(2013), p. 160.

[23] M.A. Islam, B.P. Bergsma, and C.M. Hansson, Chloride-induced corrosion behavior of stainless steel and carbon steel reinforcing bars in sound and cracked concrete, *Corrosion*, 69(2013), No. 3, p. 303.

[24] F. Zhang, J.S. Pan, and C.J. Lin, Localized corrosion behaviour of reinforcement steel in simulated concrete pore solution, *Corros. Sci*., 51(2009), No. 9, p. 2130.

[25] L. Li and A.A. Sagüés, Chloride corrosion threshold of reinforcing steel in alkaline solutions: effect of specimen size, *Corrosion*, 60(2004), No. 2, p. 195.

[26] R.D. Moser, P.M. Singh, L.F. Kahn, and K.E. Kurtis, Chloride-induced corrosion resistance of high-strength stainless steels in simulated alkaline and carbonated concrete pore solutions, *Corros. Sci*., 57(2012), No. 4, p. 241.

[27] L. Freire, M.J. Carmezim, M.G.S. Ferreira, and M.F. Montemor, The electrochemical behaviour of stainless steel AISI 304 in alkaline solutions with different pH in the presence of chlorides, *Electrochim. Acta*, 56(2011), No. 14, p. 5280.

[28] H.E. Jamil, A. Shriri, R. Boulif, M.F. Montemor, and M.G.S. Ferreira, Corrosion behaviour of reinforcing steel exposed to an amino alcohol based corrosion inhibitor, *Cem. Concr. Compos*., 27(2005), No. 6, p. 671.

[29] D.A. Koleva, J.H.W. De Wit, K. Van Breugel, Z.F. Lodhi, and E. Van Westing, Investigation of corrosion and cathodic protection in reinforced concrete: I. Application of electrochemical techniques, *J. Electrochem. Soc*., 154(2007), No. 4, p. P52.

[30] M. Saremi and E. Mahallati, A study on chloride-induced depassivation of mild steel in simulated concrete pore solution, *Cem. Concr. Res*., 32(2002), No. 12, p. 1915.

[31] Q.C. Zhang, J.S. Wu, J.J. Wang, W.L. Zheng, J.G. Chen, and A.B. Li, Corrosion behavior of weathering steel in marine atmosphere, *Mater. Chem. Phys.*, 77(2003), No. 2, p. 603.

[32] S.T. Wang, S.W. Yang, K.W. Gao, X.A. Shen, and X.L. He, Corrosion behavior and variation of apparent mechanical property of a novel low carbon bainitic steel in environment containing chloride ions, *Acta Metall. Sin.,* 44(2008), No. 9, p. 1116.

[33] M.C. García-Alonso, J.A. González, J. Miranda, M.L. Escudero, M.J. Correia, M. Salta, and A. Bennani, Corrosion behaviour of innovative stainless steels in mortar, *Cem. Concr. Res*., 37(2007), No. 11, p. 1562.

[34] Y. Qian, C. Ma, D. Niu, J. Xu, and M. Li, Influence of alloyed chromium on the atmospheric corrosion resistance of weathering steels, *Corros. Sci*., 74(2013), No. 9, p. 424.